Icarus 209 (2010) 422–433

Contents lists available at ScienceDirect

Icarus

journal homepage: www.elsevier.com/locate/icarus

A systematic spectroscopic study of eight hydrous ferric sulfates relevant to Mars

Z.C. Ling [a,b,c,*], Alian Wang [b]

[a] School of Space Science and Physics, Shandong University, Weihai, Shandong 264209, PR China
[b] Department of Earth & Planetary Sciences and McDonnell Center for the Space Sciences, Washington University in St. Louis, St. Louis, MO 63130, United States
[c] National Astronomical Observatories, Chinese Academy of Sciences, Beijing 100012, PR China

ARTICLE INFO

Article history:
Received 30 December 2009
Revised 22 April 2010
Accepted 17 May 2010
Available online 23 May 2010

Keywords:
Spectroscopy
Mars
Regoliths
Mineralogy

ABSTRACT

Ferric sulfates were observed on Mars during orbital remote sensing and surface explorations. These observations have stimulated our systematic experimental investigation on the formative conditions, stability fields, phase boundaries, and phase transition pathways of these important minerals. We report here the results from the first step of this project: eight synthesized anhydrous and hydrous crystalline ferric sulfates and their structural characters reflected through spectroscopic studies. A few phenomena observed during the 150 sets of on-going experiments for stability field study are also reported, which reveal the structural distortions that can happen under environmental conditions relevant to Mars.

© 2010 Elsevier Inc. All rights reserved.

1. Introduction

1.1. Fe-sulfates and the status variations of ferric sulfates observed on Mars

Twenty-five years ago, Clark et al. (1982) proposed that sulfates should occur on Mars based on the presence of sulfur and the oxidizing environmental conditions. The OMEGA instrument on the Mars Express and the CRISM instrument on the Mars Reconnaissance Orbiter (MRO) yielded evidence for the extensive presence of magnesium and calcium sulfates on the martian surface (Arvidson et al., 2005; Bibring et al., 2005; Gendrin et al., 2005; Langevin et al., 2005; Lichtenberg et al., 2007; Murchie et al., 2007), but less obvious and less extensive presence for Fe-sulfates (Lichtenberg et al., 2007, 2009; Milliken et al., 2007, 2008; Roach et al., 2007; Wiseman et al., 2008). In contrast, surface explorations by two Mars Exploration Rovers (MER) have found Fe-sulfates at both landing sites. Jarosite [$KFe^{3+}(SO_4)_2(OH)_6$] was identified at Meridiani Planum by the Mössbauer spectrometer (MB) on the Opportunity rover (Klingelhofer et al., 2004), and it makes ~10 wt.% in outcrop while the total sulfates make ~35 wt.% according to mineral mode calculations (based on the data from the Alpha Particle X-ray Spectrometer (APXS) by Clark et al. (2005)). It is worthwhile to note that the variations in mineral modes and chemical composition of Meridian outcrop are negligible through 17.2 km traverse (up to sol 1994) made by the Opportunity rover. At Gusev Crater, Mg-, Ca-, and Fe-sulfates were implied by compositional correlations between Mg, Ca, Fe, and S (Gellert et al., 2006; Haskin et al., 2005; Ming et al., 2006; Wang et al., 2006b,c), and their concentrations are highly heterogeneous through the exploration route of Spirit rover (Gellert et al., 2006; Haskin et al., 2005; Ming et al., 2006, 2008; Wang et al., 2008a, 2006a,b; Yen et al., 2008). Specifically, light-toned salty soils were exposed by the wheels of the Spirit rover at over 10 locations within the Columbia Hills (Rice et al., 2009; Wang et al., 2008a,b). These soils are highly enriched in S (up to 35 wt.% SO_3) as seen by APXS (Gellert et al., 2006; Ming et al., 2008; Yen et al., 2008) and contain ferric sulfates (whose identities were unclear at the current stage) as seen by MB (Morris et al., 2006, 2008). These sulfates are hydrous as seen by MiniTES (Ruff et al., 2006), and could contain Fe-sulfates such as ferricopiapite, hydronium jarosite, fibroferrite, rhomboclase and paracoquimbite based on a Pancam spectral analysis (Johnson et al., 2007) and a comparison with laboratory spectra (Lane et al., 2008). According to the mineral mode analyses (Wang et al., 2006b; Yen et al., 2008), Mg- and Ca-sulfates coexist with ferric sulfates in these soils, with highly variable proportions. More importantly, Pancam spectral changes of Tyrone yellowish soils and Kit Carson yellowish soils were observed after 175 sols' and four sols' exposure to current martian surface atmospheric conditions (Rice et al., 2009; Wang et al., 2008a). On the basis of laboratory simulations (Freeman et al., 2009; Wang et al., 2008b), the spectral change of Tyrone yellowish soils was interpreted to be potentially caused by the dehydration, amorphization, and phase transition of ferric sulfates. The observed status variations of ferric sulfates on Mars indicate that there is a different environment within the martian subsurface at shallow depth (tens of

* Corresponding author at: School of Space Science and Physics, Shandong University, Weihai, Shandong 264209, PR China.
E-mail address: zcling@sdu.edu.cn (Z.C. Ling).

0019-1035/$ - see front matter © 2010 Elsevier Inc. All rights reserved.
doi:10.1016/j.icarus.2010.05.009

centimeters, Wang et al., 2008a), which enable the presence and preservation of different hydrous salts from those in equilibrium with Mars' surface atmospheric conditions. These mission observations stimulated our laboratory investigation for the stability field, the phase boundaries, the pathways of phase transitions, and the dehydration and rehydration rates of hydrous salts. This type of fundamental knowledge on sulfates will help us to link the mission observations of hydrous salts to the hydrological evolution and current water budget on Mars.

In order to understand the origin and the formative conditions of martian sulfates, laboratory experiments have been conducted for Mg-sulfates, Ca-sulfates, and their mixtures, on their phase boundary, stability fields, phase transition pathways, and the reaction rates of dehydration and rehydration processes (Chipera and Vaniman, 2007; Chou et al., 2002; Vaniman and Chipera, 2006; Wang and Freeman, 2009; Wang et al., 2006a, 2009), while the same types of knowledge on Fe-sulfates, especially ferric sulfates, are largely lacking at present.

On Earth, Fe-sulfate minerals often occur in acid mine drainages, which are extremely heterogeneous and complex systems (Alpers et al., 2000). Fe-sulfates can occur in the forms of ferrous and ferric sulfates, with differences in hydration degree and acidity states. The evolution from Fe-sulfides to ferrous or ferric sulfate minerals to iron oxyhydroxide and oxide minerals occurs through a series of hydrolysis, oxidation, dehydration, and neutralization processes (Jerz and Rimstidt, 2003). Among this chain of Fe-bearing minerals, we chose to concentrate our study on ferric (Fe^{3+}) sulfates (the acidic weathering products of basaltic materials in an oxidizing environments, e.g., Mars), and especially normal ferric sulfates, thus to limit the variables in our experiments.

We report here the first step of a series of experimental investigations, in which we synthesized seven ferric sulfates in the laboratory (Table 1). The conditions (*T*, RH, and initial chemistry) during the synthesis provided a first order understanding of the formative conditions and the meta-stability field of individual ferric sulfate. Using five of the seven synthesized ferric sulfates, we have started 150 sets of experiments to investigate their stability fields. While these experiments are on-going, we report here a few interesting observations derived from the experiments.

XRD, Raman, Mid-IR, and Vis–NIR spectroscopy are the main technologies used in this study. The structures and the purities of synthesized ferric sulfates were first confirmed by XRD, then Raman, Mid-IR, and Vis–NIR spectra were obtained from them. The obtained standard Raman spectra are being used for non-invasive phase identifications of the reaction products at intermediate stages of 150 sets of experiments for stability field study (Freeman et al., 2009; Wang et al., 2008b). In addition, the obtained standard Raman, Mid-IR and Vis–NIR spectra of synthetic pure ferric sulfates will be used for the interpretation of data from missions to Mars (OMEGA, CRISM, Pancam, and future Raman system on ExoMars rover). Our goal is to build links between orbital remote sensing and surface exploration through detailed laboratory experiments, for the purpose of gaining a comprehensive understanding of the large scale stratigraphic distribution of martian sulfates on the basis of local mineral assemblages that are consistent with thermodynamics and kinetics, thus hydrological evolution models can be developed.

2. Experimental procedures

2.1. Synthesis of ferric sulfates

2.1.1. Crystallization from saturated solutions

A single batch of saturated aqueous solution of ferric sulfate was prepared by dissolving $Fe_2(SO_4)_3{\cdot}xH_2O$ (supplier Alfa Aesar, Ward Hill, MA) into water. We synthesized rhomboclase ($FeH(SO_4)_2{\cdot}4H_2O$) by adding 0.6 g of 98% H_2SO_4 into 4 g of the saturated solution. The uncovered beaker that holds the solution was left under ambient conditions in laboratory ($T \sim 21$ °C, RH < 50%), white colored powder precipitated after about 1 week. The powder sample was washed in ethanol to remove the remaining acid. The sample was first identified by XRD to be pure rhomboclase, then checked by multi-spots Raman measurement for its homogeneity.

When using only 0.3 g of sulfuric acid in the above saturated aqueous solution, ferricopiapite and paracoquimbite would first crystallize after 3 days, and then change into a mixture of paracoquimbite and rhomboclase. The purple clusters of paracoquimbite were picked out for XRD and Raman measurements.

We used a humidity-buffer technology (Chou et al., 2002) to synthesize and stabilize several ferric sulfates of different hydration states at fixed temperature (*T*) and relative humidity (RH) conditions. The humidity buffers we used are based on saturated aqueous solutions of the binary salts LiBr, LiCl, $MgCl_2$, $Mg(NO_3)_2$, NaBr, KI, NaCl, KCl, KNO_3, and pure water (Chou et al., 2002; Greenspan, 1977), that covers 6–100% RH in temperature range 50–5 °C. We synthesized ferricopiapite by holding the saturated ferric sulfate solution at 50 °C using the KI humidity buffer, which yielded relative humidity of about RH 65%. After 3 days, a yellowish granular blocky phase had precipitated out, which was washed by ethanol to remove the remaining acid in the precipitates (ferricopiapite).

2.1.2. Crystallization from a commercial amorphous ferric sulfate

A commercial amorphous ferric sulfate (Acros Organics, Geel, Belgium) was also used as the starting material to make more ferric sulfates of different structures. After heating at 200 °C in air for 3 days, the original yellow colored powder changed its color to a pale yellow. XRD analysis of this product indicated that it became crystalline mikasaite, an anhydrous phase [$Fe_2(SO_4)_3$]. The gravimetric measurements before and after heating confirmed that the original amorphous phase had five structural waters, i.e., it was a pentahydrous amorphous ferric sulfate.

When amorphous pentahydrous ferric sulfate was put into a KI humidity buffer at 95 °C (~60% RH) for 1 day, it converted to crystalline kornelite ($Fe_2(SO_4)_3{\cdot}7H_2O$) with a pinkish purple color.

Table 1
Ferric sulfates studied by Raman and XRD in this study, and the data available in Rruff database.

Phase	Formula	Space group	Rruff_XRD	Rruff_Raman	Our XRD	Our Raman
Mikasaite	$Fe_2(SO_4)_3$	$\bar{R}3$	No	No	Yes	Yes
Amorphous (5w)	$Fe_2(SO_4)_3{\cdot}5H_2O$	No	No	No	Yes	Yes
Pentahydrate	$Fe_2(SO_4)_3{\cdot}5H_2O$	$P2_1/m$	No	Yes	Yes	Yes
Hexahydrate	$Fe_2(SO_4)_3{\cdot}6H_2O$	Unknown	No	No	Yes	Yes
Kornelite	$Fe_2(SO_4)_3{\cdot}7H_2O$	$P2_1/n$	No	No	Yes	Yes
Paracoquimbite	$Fe_2(SO_4)_3{\cdot}9H_2O$	$\bar{R}3$	Yes	Yes	Yes	Yes
Rhomboclase	$FeH(SO_4)_2{\cdot}4H_2O$	Pnma	No	Yes	Yes	Yes
Ferricopiapite	$Fe_{4.67}(SO_4)_6(OH)_2{\cdot}20H_2O$	$\bar{P}1$	Yes	Yes	Yes	Yes

When putting the produced crystalline kornelite into a LiCl humidity buffer at 95 °C (~10% RH) for one more day, it changed into a phase with a light pinkish color, which has five structural waters revealed by gravimetric measurement, but has a crystalline structure ($Fe_2(SO_4)_3{\cdot}5H_2O$). When the amorphous pentahydrous ferric sulfate was put into a NaI humidity buffer at 95 °C (~23% RH), it produced pale yellow colored crystals. This phase has different XRD and Raman spectral patterns from those of kornelite and pentahydrate. The gravimetric measurement suggests that it has six structural waters. It is called "hexahydrate" in the tables and figures of this paper, and will be discussed later.

2.2. XRD and Raman, Mid-IR, Vis–NIR spectroscopic measurements of synthetic ferric sulfates

An XRD pattern of each synthesized ferric sulfate was taken for the purpose of confirming its identity, including those potentially polymorphous structures. The choice of spectroscopic measurements used in this study is based on their usefulness in our next set of experiments for stability field study and on the fact that they are either conventionally used in planetary missions, or are being selected for future mission to Mars.

It is worthwhile to note that Raman, Mid-IR, and NIR spectra are inter-related by the vibrational transitions of a molecule or ionic entities in a mineral structure, but represent different aspects of this process. Therefore, a combined study using these spectra will provide a comprehensive understanding of the structural and compositional character of the studied species.

A Rigaku Geigerflex X-ray diffractometer with a Cu Kα radiation source was used. The synthetic ferric sulfate samples were first checked by multi-spots Raman measurement on their homogeneity, then about 0.2–0.3 g of each sample was quickly ground together with CaF_2 powder (as an internal standard) for the collection of a powder XRD pattern. Multi-spots Raman spectra of the XRD sample were collected again after each XRD measurement, which showed that, for all hydrous ferric sulfates that we studied, no detectable phase change occurred during the course of the XRD measurements.

A HoloLab5000-532 laser Raman spectrometer (Kaiser Optical Systems Inc.) was used to obtain Raman spectra of the samples from 150 to 4000 cm^{-1}. A 20× microscopic objective (NA = 0.4) was used to focus the laser beam (~6 μm in diameter) of 532 nm wavelength onto the sample and to collect the Raman photons produced by the sample. Each measurement typically uses 2 s exposure time and 16 accumulations to get a Raman spectrum with good signal/noise ratio for each ferric sulfate sample.

A Nicolet Nexus 670 Fourier transform infrared interferometer (FTIR) spectrometer was used to make Mid-IR ATR (attenuated total reflectance) measurements (2.5–25 μm) of ferric sulfate samples, using a diamond anvil ATR accessory (Harrick Scientific). NIR Diffuse reflectance spectra (1–5 μm) were measured by using a Cricket accessory (Harrick Scientific) on the same FTIR spectrometer. A gold-coated rough surface was used as the reflectance standard. The Nicolet Nexus 670 FTIR spectrometer is purged constantly using dry-N_2 in order to remove adsorbed water from the samples. An Analytical Spectral Device (ASD Inc.) was used to obtain the Vis–NIR reflectance spectra (0.35–2.5 μm) of all ferric sulfates, and a halon plate was used as the reflectance standard.

The peak positions in Raman, MIR, and Vis–NIR spectra were obtained by spectral deconvolution procedure of GRAMS 32 software package (Thermo Scientific), with mixed Gaussian–Lorentzian peak shape, linear baseline subtraction, and the constrain-free iteration option for fitting all parameters until convergence (or a minimum) was attained.

3. Results and discussion

3.1. Crystal structure of three selected ferric sulfates

We choose three ferric sulfates, pentahydrite, kornelite and paracoquimbite, to discuss their crystal structures and to support their spectral characterizations. We made a polygonal drawing for each structure (Fig. 1) using software Diamond 2.1 (Crystal Impact, 1998–2002) based on data from the American Mineralogist Crystal Structure Database.

Within these ferric sulfates, the SO_4 tetrahedra are connected to Fe cations in different ways, either by sharing an oxygen as coordinator for polyhedra, or by hydrogen bonding. As shown in Fig. 1a, the pentahydrate structure of $Fe_2(SO_4)_3{\cdot}5H_2O$ (Majzlan et al., 2005) contains two sets of crystallographically distinct SO_4 tetrahedra. One set shares three bridging O atoms with the neighboring Fe^{3+} octahedra, while the other set shares only two. Three different water positions exist in a unit cell of $Fe_2(SO_4)_3{\cdot}5H_2O$ (Fig. 1a), and all are at the corners of Fe octahedra. Different from pentahydrate, the kornelite structure (Robinson and Fang, 1973) possesses three sets of distinct SO_4 tetrahedra (Fig. 1b). Every SO_4 tetrahedron in kornelite shares two bridging O atoms with the neighboring Fe^{3+} octahedra. As indicated by Fig. 1b, six of all the eight different water positions in kornelite appear as corners of Fe^{3+} octahedra. The other two water positions connect to either Fe^{3+} or S cations by hydrogen bonding only, thus these can be regarded as "free" waters in the structure of kornelite. The polyhedral representation of paracoquimbite is shown in Fig. 1c. There are two sets of distinct SO_4 tetrahedra in the structure of paracoquimbite (Robinson and Fang, 1971), each SO_4 tetrahedron shares two O atoms with neighboring Fe^{3+} octahedra. There are six different water sites in paracoquimbite, and two are "free" waters in the structure. Considering their important roles in vibrational spectra, we list the S–O lengths and O–S–O angles among SO_4 tetrahedra in the three structures in Table 2.

3.2. Hexahydrate ferric sulfate suggested by XRD, gravimetry, and synthesizing conditions

The identities of seven crystalline ferric sulfates were confirmed by corresponding XRD patterns in the PDF2006 database. Most of the synthesized ferric sulfates are pure, except for paracoquimbite and ferricopiapite, which contain trace amounts of rhomboclase. Fortunately, we could pick out the grains with a specific color to collect them as the major phase in a sample for XRD and Raman measurement to get their characteristic patterns.

A pale yellowish powder produced by keeping amorphous pentahydrous ferric sulfate at 95 °C and ~23% RH produces a distinct XRD pattern with no match in the PDF 2006 database. It is a phase different from either the ferric sulfates synthesized by us or any other ferric sulfates in the PDF2006 database. Our gravimetric measurement suggests that this phase has a molecular formula roughly $Fe_2(SO_4)_3{\cdot}5.75H_2O$. Compared with the relative humidity conditions we used to form kornelite (~60% RH) and to form pentahydrate (~11% RH), this phase was synthesized at an intermediate relative humidity level ~23% RH from the same starting amorphous pentahydrated ferric sulfate, thus we anticipate it may hold an intermediate number of structural water molecules between kornelite and pentahydrate, e.g. a hexahydrate. Further experiments demonstrated that this phase could dehydrate into pentahydrate when kept long enough in a NaI humidity buffer at 95 °C (~23% RH). Therefore, we tentatively ascribe this phase as a ferric sulfate containing six structural water molecules ($Fe_2(SO_4)_3{\cdot}6H_2O$). Majzlan et al. (2005) has made a crystal structure refinement of a pentahydrate ferric sulfate and argued that

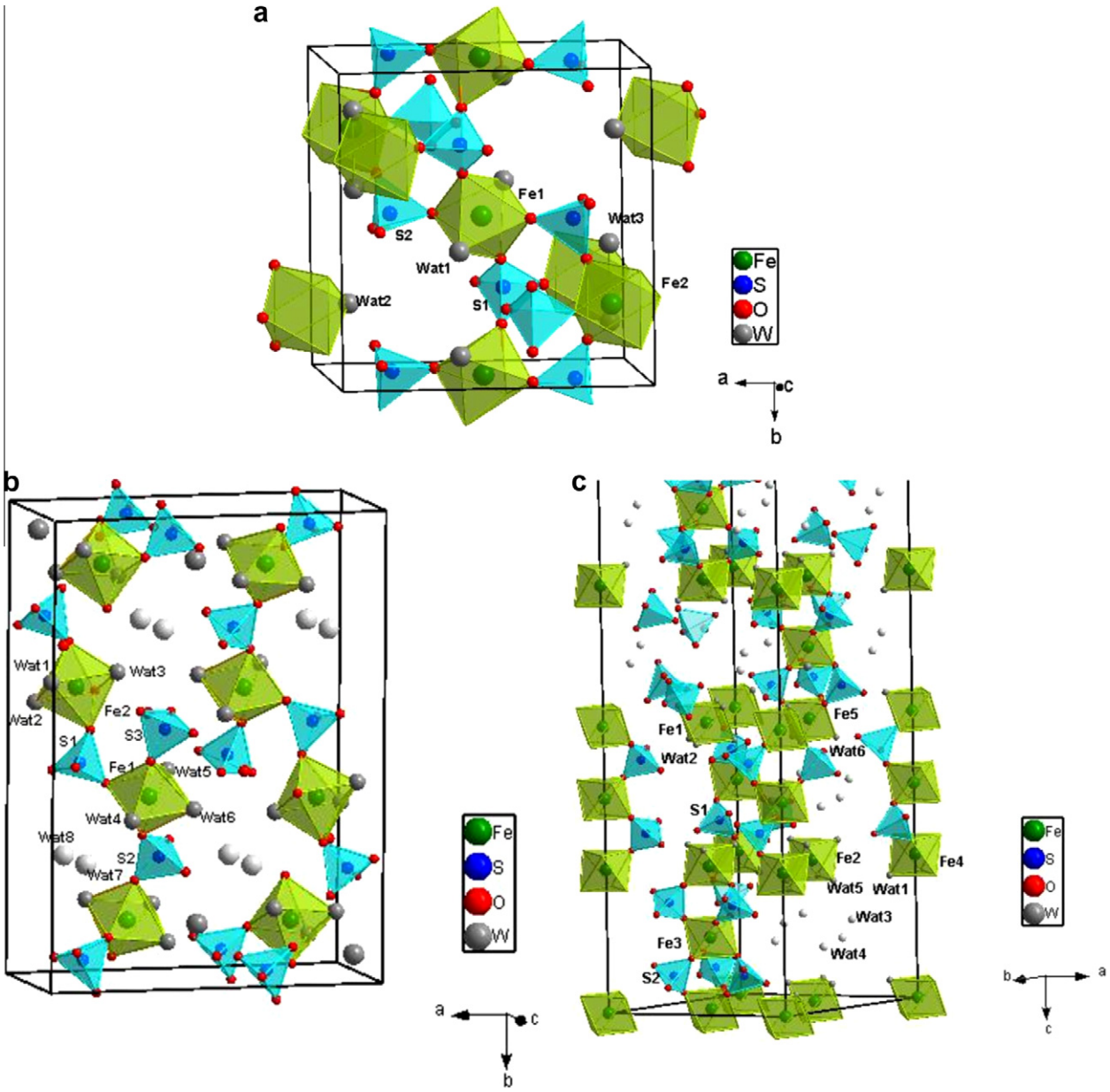

Fig. 1. Polygonal drawings of three hydrated ferric-sulfate structures: (a) pentahydrate; (b) kornelite; (c) paracoquimbite (only show ½ of a unit cell).

Table 2
Comparisons of bond length and angles in SO_4 tetrahedra of pentahydrate, kornelite and paracoquimbite.

Ferric sulfate	Tetrahedron	Average lengths (Å)	Δ_{length} (Å)	Average angles (°)	Δ_{angle} (°)
Pentahydrate	$S(1)O_4$	1.446 (6)	0.039 (1)	109.2 (8)	11.1 (8)
	$S(2)O_4$	1.457 (7)	0.037 (2)	109.3 (6)	14.6 (5)
Kornelite	$S(1)O_4$	1.466 (1)	0.060 (7)	109.4 (4)	6.5 (4)
	$S(2)O_4$	1.457 (3)	0.056 (2)	109.4 (4)	7.2 (0)
	$S(3)O_4$	1.471 (9)	0.034 (0)	109.4 (5)	5.4 (0)
Paracoquimbite	$S(1)O_4$	1.473 (4)	0.031 (7)	109.4 (7)	2.4 (7)
	$S(2)O_4$	1.479 (9)	0.056 (1)	109.4 (7)	2.9 (2)

pentahydrite should be called "lausenite", because they have not found a structure with six structural waters. We argue that ferric sulfate with six structural waters does exist, and the pale yellowish phase synthesized by us could be called hexahydrate ferric sulfate. Structural refinement of our newly found species will be conducted in order to validate our statement.

3.3. Raman spectral analysis

3.3.1. Raman spectra of eight ferric sulfates

Raman spectra were taken from eight synthetic ferric sulfates (seven crystalline and one amorphous). These spectra are split into three spectral regions in Fig. 2: from 150 to 1500 cm^{-1}

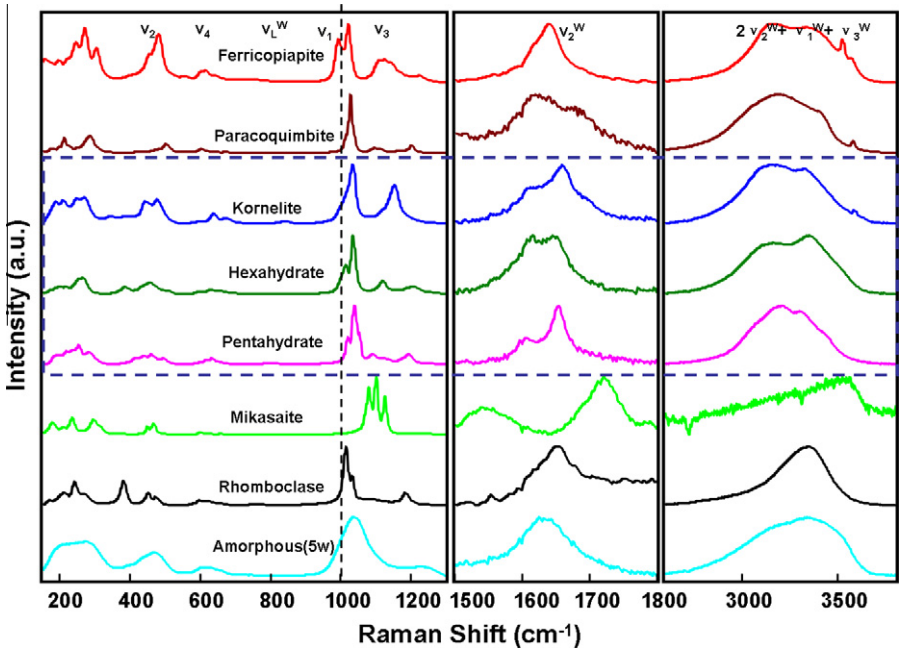

Fig. 2. Raman spectra of eight synthesized anhydrate and hydrated ferric sulfates: ranges from 150 to 1500 cm^{-1} (SO_4 tetrahedra internal and external vibrations), 1500 to 1800 cm^{-1} (water bending vibrations), and 2600 to 3800 cm^{-1} (water stretching vibrations), are shown separately.

corresponding to the region of SO_4 tetrahedra internal and external vibrations, 1500 to 1800 cm^{-1} for water bending vibration, and 2600 to 3800 cm^{-1} for water stretching vibrations, respectively.

The Raman peaks in the first spectral region (150–1500 cm^{-1}) are contributed by the fundamental vibrational modes from the SO_4 tetrahedra in Fe-sulfates, including both internal and external modes. The $[SO_4]^{2-}$ tetrahedra exhibit symmetric stretching (v_1) and bending (v_2) modes, and asymmetric stretching (v_3) and bending (v_4) modes at 983, 450, 1105, and 611 cm^{-1}, respectively (Nakamoto, 1986). All four fundamental modes of $[SO_4]^{2-}$ are Raman active, while only asymmetric stretching (v_3) and bending (v_4) are IR active. The symmetric vibrations (v_1, v_2) produce more intense peaks than the asymmetric ones (v_3, v_4) in Raman spectra. As indicated by a dashed line in Fig. 2, the v_1 peaks of different ferric sulfates shift from low wavenumber (989 cm^{-1} for ferricopiapite) to high wavenumber (1099 cm^{-1} for mikasaite), following a trend of reduction of degree of hydration of these ferric sulfates. The shift of the Raman v_1 peak positions following the same trend was observed in hydrous Mg-sulfates and Ca-sulfates: i.e., more structural water molecules in a crystal framework would increase the hydrogen bonding effect on SO_4 tetrahedra, thus decreasing their vibrational energy. All eight synthetic ferric sulfates show the strongest diagnostic peak patterns in the v_1 peak region, which makes this region very useful for ferric sulfate phase identification from the spectra of mixtures.

In addition to the v_1 peak position, the v_1 peak shapes also reflect the structural differences of these ferric sulfates. For example, the v_1 peak for kornelite appears broader than those of pentahydrate and paracoquimbite, because kornelite has three crystallographically distinct SO_4 tetrahedra compared with two distinct types of SO_4 tetrahedra in the other two structures (Table 2). A generally shorter S–O bond length contributes a larger force constant and thus has higher energy. Therefore, pentahydrate with a shorter average bond length has higher v_1 peaks than those of kornelite and paracoquimbite. The v_1 peak of pentahydrate splits into three peaks at 1036.4, 1051.5 and 1017.0 cm^{-1} respectively, while the v_1 peak of paracoquimbite appears as one sharp peak at 1025.4 cm^{-1} with two weak shoulders. This feature suggests a smaller distortion of the SO_4 tetrahedra in paracoquimbite structure than that in pentahydrate. The SO_4 tetrahedra distortions in three structures are shown in Table 2. For example, paracoquimbite possesses a smaller variation in O–S–O angles (Δ = 2.4–2.9°) within its SO_4 tetrahedra (Robinson and Fang, 1971), whereas the O–S–O angle variations in pentahydrite vary in a much large range (Δ = 11.1–14.6°) (Majzlan et al., 2005).

H_2O and OH in the crystal structures of hydrous ferric sulfates contribute characteristic peaks in Raman spectra (1500–1800 cm^{-1} and 2600–3800 cm^{-1} spectral ranges). The liquid H_2O molecule has a symmetric H–O–H stretching (v_1) mode at 3450 cm^{-1}, an asymmetric H–O–H stretching (v_3) mode at 3615 cm^{-1}, an H–O–H bending (v_2) mode at 1640 cm^{-1}, respectively (Nakamoto, 1986). Accordingly, the spectral peaks related to structural water in ferric sulfates can be assigned. Although Raman and Mid-IR peaks contributed by water bending modes (~1600 cm^{-1}) are weak, they are still diagnostic enough to distinguish different ferric sulfates (Fig. 2, 1500–1800 cm^{-1}).

The broad Raman peaks in the 2600–3800 cm^{-1} spectral region (Fig. 2) are contributed by three vibrational modes of structural water in these ferric sulfates: the symmetric stretching mode (v_1), the weaker asymmetric stretching mode (v_3), and the 1st overtone of the bending mode ($2v_2$). These peak positions and peak shapes reflect different hydration degrees of the samples. Specifically, ferricopiapite ($Fe_{4.67}(SO_4)_6(OH)_2{\cdot}20H_2O$) has both structural water and hydroxyl, thus its spectrum in this region shows two sharp peaks, 3523.2 and 3571.8 cm^{-1}, very typical for the stretching mode of OH bonding, sitting on the wing of a broad peak from structural water (Fig. 2), Kornelite and paracoquimbite, each also has a similar sharp peak (3586.9 and 3577.3 cm^{-1} respectively) although they are not OH-bearing. In addition, those sharp peaks appear in the Mid-IR and NIR spectra of these three ferric sulfates. A minor impurity in kornelite and paracoquimbite is a potential reason, while structural distortion of some water molecules (eight distinct types in kornelite and six in paracoquimbite) cannot be excluded. In the spectrum of anhydrous mikasaite, water peaks in the 2600–3800 cm^{-1} and in 1500–1800 cm^{-1} spectral ranges are observable but extremely weak, the peak positions and shapes

suggest that they are contributed by the water molecules adsorbed at the grain surfaces of mikasaite. The Raman peaks of eight synthetic ferric sulfates and their assignments are listed in Table 3.

3.3.2. Comparison of the Raman spectra from kornelite, hexahydrate, and pentahydrate

We compare the Raman spectrum of newly found hexahydrate ferric sulfate with those of septahydrate (kornelite) and pentahydrate in Fig. 2 and Table 3. The symmetric stretching vibration v_1 mode of SO_4 tetrahedra in kornelite is a broad peak located at 1032 cm^{-1}; the similar peak splits into two peaks at 1032 and 1012 cm^{-1} for hexahydrate, and into three peaks at 1051, 1038, and 1018 cm^{-1} for pentahydrate, respectively. Differences in v_1 peak splitting suggest variation in SO_4 tetrahedral distortion in their crystal structures, i.e., the larger the distortion, the more v_1 peak splitting that would be expected (consistent with the structural features of kornelite and pentahydrate). This is also supported by the fact that most of the other vibrational modes for SO_4 tetrahedra (v_2, v_3, v_4) tend to have multiple peaks following the decreasing of their hydration states. Therefore, we suggest that hexahydrate has a medium distortion of SO_4 tetrahedra among the three ferric sulfates. Kornelite and pentahydrate have librational modes of H_2O near 800 cm^{-1}, while hexahydrate does not show this peak, suggesting a restriction of water molecules in this hexahydrate structure.

As shown in the 1500–1800 cm^{-1} region of Fig. 2, the peak widths for the water bending mode appear gradually reduced as the hydration state decreases from kornelite to pentahydrate (~97 cm^{-1} for kornelite, ~89 cm^{-1} for hexahydrate and ~51 cm^{-1} for pentahydrate). For the water stretching modes in the 2600–3800 cm^{-1} range, it is easy to see that the width of water peak of hexahydrate and septahydrate (kornelite) are larger than that of pentahydrate, due to the higher hydration states. The relative intensity of asymmetric stretching modes (~3350 cm^{-1}) of H_2O is higher than that of overtones of bending modes ($2v_2$, ~3130 cm^{-1}) for kornelite. However, reversed relative intensities were observed for hexahydrate, which indicate a different lattice environment for structural waters in hexahydrate.

3.4. Mid-IR (ATR) spectral analysis

Mid-IR attenuated total reflectance (ATR) spectra (400–4000 cm^{-1}) for our eight synthetic ferric sulfates (Fig. 3) were taken in order to support the Raman spectral analyses and peak assignments. In general, Mid-IR spectral peaks of those ferric sulfates have wider peak widths and weaker peak intensities compared with their respective Raman spectra. It is interesting to note that the Mid-IR spectral patterns of these ferric sulfates in 1500–1800 cm^{-1} and 2500–4000 cm^{-1} regions are quite similar to those in Raman spectra, because the stretching and bending vibrational modes of water in these sulfates are both Raman and IR active. In the spectral region of 400–1400 cm^{-1}, the asymmetric stretching vibrational mode (v_3) of SO_4 contributes the strongest IR peak. This peak splits into several sub-peaks in Mid-IR spectra of these ferric sulfates, caused by large distortion of SO_4 tetrahedra in their structures. In addition, IR peaks at similar positions of Raman active v_1 mode also appear, due to the break-down of the spectral selection rule by (again) the large distortions of SO_4

Table 3
Raman peak positions (in cm^{-1}) of eight synthesized hydrous and anhydrous Fe-sulfates. (Bold numbers are the strongest v_1 peak for each ferric sulfates derived by peak fitting.)

Sample	H_2O mode			SO_4 vib. modes				Others
	Stretching	Bending	Librational	v_1	v_2	v_3	v_4	
Ferricopiapite	3143.2 3377.7 3523.2 3571.8	1612.7 1638.9	751.8 835.7	**989.4** 1002.7 1019.1	451.8 467.0 480.5	1104.9 1123.9 1141.9 1150.5 1222.3	599.4 614.8 636.5	244.0 270.0 302.9
Paracoquimbite	3046.1 3244.8 3411.5 3577.3	1620.3 1681.8	876.9	1012.3 **1025.4** 1037.0	477.7 501.5 514.1	1092.6 1112.1 1170.2 1199.7	601.9 628.1 674.8	211.1 285.6
Kornelite	3122.8 3352.2 3586.9	1613.4 1658.3 1696.3	838.0	992.7 1021.3 **1032.9**	439.3 452.1 476.2	1078.4 1124.2 1150.5 1181.7	596.7 635.8 671.5	187.2 208.8 247.9 268.8
Hexahydrate	3132.3 3362.4 3498.9	1613.0 1651.1		1000.7 1011.8 **1032.8**	434.4 455.3 468.3 508.2	1116.7 1199.9	596.3 626.8 655.2	264.4 384.3
Pentahydrate	3057.4 3195.4 3323.3 3425.4	1604.7 1652.6	798.6	1017.0 **1036.4** 1051.5	415.5 440.9 457.3 467.5 493.9	1086.6 1119.0 1189.2	598.8 614.2 631.1 652.0	253.1 280.8
Mikasaite				1040.3 1068.6 1077.9 **1097.9**	448.1 461.2 468.1	1123.4	600.1 612.9 627.8 657.1 676.7	178.1 233.8 294.9
Rhomboclase	3191.6 3348.6	1647.8	735.5 761.4 775.3	**1011.8** 1030.8	440.1 450.9 472.6	1066.0 1182.7	595.2 620.3 652.6	240.9 379.9
Amorphous (5w)	3180.4 3397.5 3520.8	1633.8		992.9 **1035.4**	424.2 472.2	1089.0 1230.6	597.7 627.6 659.1	198.7 276.6

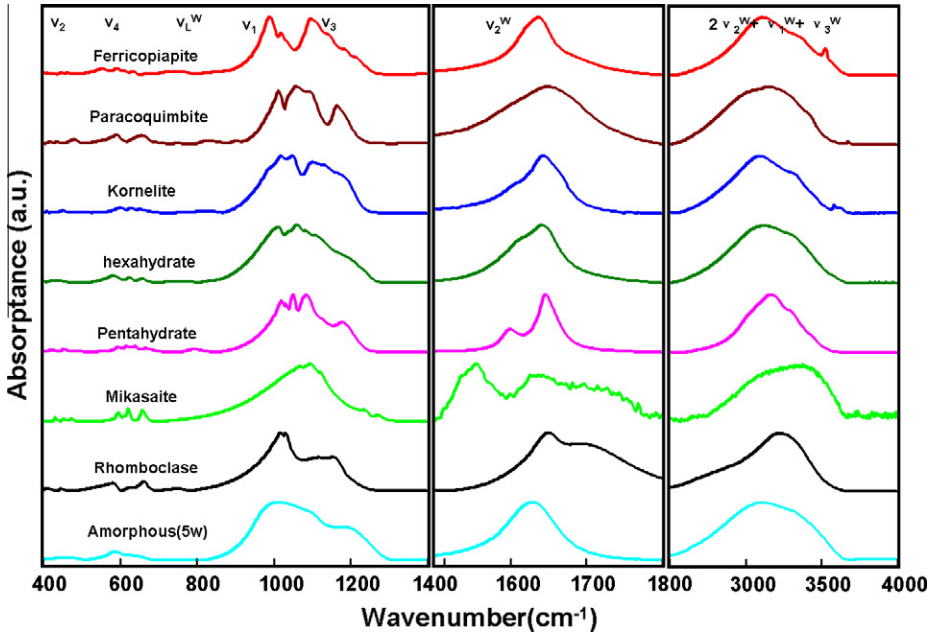

Fig. 3. Mid-IR (ATR) spectra of eight synthesized anhydrous and hydrous ferric sulfates, ranges from 400 to 1400 cm^{-1} (SO_4 tetrahedra internal vibrations), 1500 to 1800 cm^{-1} (water bending vibrations), and 2500 to 4000 cm^{-1} (water stretching vibrations), respectively.

tetrahedra in the structures. The combination of the v_3 peak splitting and the appearance of the v_1 peak produces very complicated Mid-IR spectral patterns in the 900–1200 cm^{-1} spectral range, with broadened and overlapping sub-peaks (Fig. 3), which are

Table 4
Mid-IR (ATR) peaks (in cm^{-1}) and the assignments of eight synthesized hydrous and anhydrous Fe-sulfates.

Sample	H_2O modes			SO_4 vib. modes				Others
	Stretching	Bending	Librational	v_1	v_2	v_3	v_4	
Ferricopiapite	3121.7 3373.1 2885.9 3540.1 3524.1	1631.6 1638.7 1700.1	749.0	976.7 990.7 1018.3 1031.4	445.6 463.8	1093.8 1145.2 1208.7 1114.2 1182.5	590.9 610.2 633.7	2320.7
Paracoquimbite	3036.8 3162.2 3314.2 3429.9 3675.3	1561.3 1651.2	831.7 900.4	994.9 1011.8 1052.7	480.7	1093.3 1161.0 1177.0	590.9 656.7	
Kornelite	2789.0 3095.7 3337.0 3585.1 3621.5	1609.2 1645.5 1673.2	827.2	992.1 1020.7 1050.2	451.4	1093.0 1129.6 1180.1	601.2 628.3 651.1	2402.0
Hexahydrate	2850.3 3091.9 3340.4	1628.9 1647.3	750.6	977.5 988.5 1010.1 1037.1 1057.4	428.1 436.0	1082.8 1108.1 1187.7 1233.3	583.6 625.7 658.1	2393.0
Pentahydrate	3029.9 3187.4 3311.1 3391.5	1598.3 1648.1	793.9	1003.7 1019.3 1031.4 1048.7	421.0 453.9	1069.8 1084.3 1123.2 1180.8	594.9 616.4 638.8 666.0	2389.0
Mikasaite	3179.5 3448.2			1068.0 1083.0 1093.0	432.2 454.1 474.0	1119.0 1234.0 1270.0	595.1 609.4 621.2 658.6	2167.4 2338.2
Rhomboclase	2953.4 3179.4 3334.8	1644.0 1707.6	751.2	968.7 1016.6 1032.5	409.7 415.9 447.0	1114.8 1162.1	581.6 629.8 662.5	2168.6
Amorphous (5w)	3096.6 3394.8	1626.4		995.3	459.3	1093.8 1201.3	586.7 626.0 650.4	

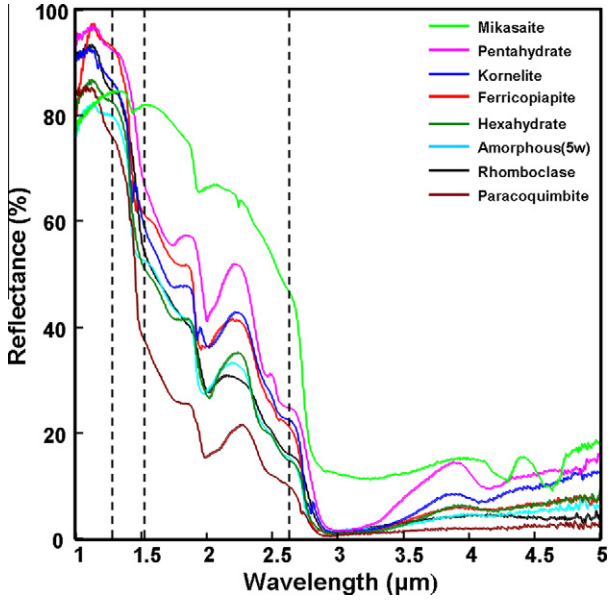

Fig. 4. NIR diffuse reflectance spectra (1–5 μm) of eight ferric sulfates.

characteristic for these eight ferric sulfates to be distinguished from each other. It is interesting to note that the adsorbed water on mikasaite grain surfaces appears to be more evident in the IR spectrum than in its Raman spectrum. The Mid-IR peaks of eight ferric sulfates and their assignments are listed in Table 4.

3.5. NIR diffusion reflectance spectral analysis

Near-IR (1–5 μm) diffuse reflectance spectra of eight synthetic ferric sulfates were taken (Fig. 4) for the purpose of investigating the overtone and combinational vibrational modes from H_2O, OH, and SO_4 ionic groups. The assignments for the spectral peaks in this range were made based on the peak assignments in Raman and Mid-IR spectra for fundamental vibrational modes. According to these assignments, the 1–5 μm NIR spectral regions can be roughly divided into four sections: (1) peaks in wavelength region $\lambda < 1.33$ μm belong to high order overtones and combination modes of water vibrations, such as $(\nu_1 + \nu_2 + \nu_3)^{w}$ (the superscript "w" denotes vibration modes from waters); (2) the peaks in wavelength region $1.33 < \lambda < 1.52$ μm attributed to the first overtone of the fundamental stretching modes of water, such as $2\nu_1^{w}$ or $2\nu_3^{w}$; (3) the $1.52 < \lambda < 2.63$ μm region attributed to the combination modes of water, such as $\nu_2^{w} + \nu_1^{w}$ (or ν_3^{w}) and $2\nu_2^{w} + \nu_1^{w}$ (or ν_3^{w}), as well as the combinational modes of water and SO_4, such as $(\nu_1 + \nu_3)^{SO4} + \nu_2^{w}$, ν_1^{w} (or ν_3^{w}) $+ \nu_3^{SO4}$, etc.; (4) the >2.63 μm region attributed to stretching fundamentals (ν_1^{w} and ν_3^{w}), first overtone of bending ($2\nu_2^{w}$) of water, and the combination mode of SO_4 ($(\nu_1 + \nu_3)^{SO4}$), etc. (Frost et al., 2005; Cloutis et al., 2006, 2008; Freeman et al., 2008; Liu et al., 2009).

It is interesting to find that in 1.52–5 μm region, highly hydrated ferric sulfate, such as paracoquimbite, has the lowest albedo, while the driest phase mikasaite has the highest albedo. Focusing on the 2.4–2.6 μm spectral region that is diagnostic for polyhydrated sulfates, ferricopiapite (with the highest degree of hydration) has three peaks at 2.41, 2.46 and 2.54 μm, while the other phases have only two peaks that can be visually resolved. This phenomenon indicates that ferricopiapite has more distinct crystallographic sites for water molecules than for the other phases. In the NIR region from 1 to 2.5 μm, kornelite shows three prominent diagnostic absorption features at 1.43, 1.92, and 2.01 μm. The similar spectral features of ferricopiapite shift to 1.45, 1.95 and 1.98 μm. These absorption bands would be appreciable for the detection of these phases by remotely sensed data. The detailed assignments of the peaks are shown in Table 5.

3.6. Vis–NIR reflectance spectral analysis

The Vis–NIR reflectance spectra (0.35–2.5 μm) were taken from eight synthetic ferric sulfates, but only the spectral region from 0.35 to 1.25 μm is shown in Fig. 5 (spectral features in spectral range from 1.0 to 2.5 μm are discussed in Section 3.4). Electronic transitions of Fe^{3+} (best described by crystal field theory, Burns, 1993) are the major contributors of the spectral bands in this region. For the eight synthetic ferric sulfates, the three major Fe^{3+} bands are: a broad band centered from 0.703 to 0.868 μm that is associated with the $^6A_{1g} \rightarrow {}^4T_{1g}$ transition; a second broad band centered from 0.531 and 0.572 μm that is contributed by $^6A_{1g} \rightarrow {}^4T_{2g}$ transition; and a narrower band centered near 0.43 μm caused by the $^6A_{1g} \rightarrow (4A_{1g}, {}^4E_g)$ transitions (Burns, 1993; Hunt and Ashley, 1979). The center positions of these Vis–NIR bands of eight ferric sulfates and their assignments are listed in Table 6.

Table 5
Center position of absorption bands (in μm) in NIR diffuse reflectance spectra (1–5 μm) for the eight synthesized ferric sulfates and the assignments.

Ferr	Para	Kor	Hex	Pen	Mik	Rhom	Amor	Assignment
					4.63			$(\nu_1 + \nu_3)^{SO4}$
4.20		4.10	4.20	4.16	4.26		4.18	$(\nu_1 + \nu_3)^{SO4}$
2.95	2.95	2.95	2.94	2.97	3.25	2.92	2.91	$2\nu_2^{w}$, ν_1^{w}, ν_3^{w}
2.83	2.72	2.79			2.89			$2\nu_2^{w}$, ν_1^{w}, ν_3^{w}
		2.76						$2\nu_2^{w}$, ν_1^{w}, ν_3^{w}
2.54	2.57	2.56	2.59	2.57		2.59	2.56	$(\nu_1 + \nu_3)^{SO4} + \nu_2^{w}$
2.46	2.46					2.44		$(\nu_1 + \nu_3)^{SO4} + \nu_2^{w}$
2.41		2.41	2.40	2.43			2.40	$(\nu_1 + \nu_3)^{SO4} + \nu_2^{w}$
2.21					2.24			ν_1^{w} (or ν_3^{w}) $+ \nu_3^{SO4}$
2.01	2.06					2.07		$\nu_2^{w} + \nu_1^{w}$ (or ν_3^{w})
1.98	1.98	2.01	2.01	2.05	1.94	2.00		$\nu_2^{w} + \nu_1^{w}$ (or ν_3^{w})
1.95s			1.96	2.00				$\nu_2^{w} + \nu_1^{w}$ (or ν_3^{w})
	1.91	1.92			1.93		1.97	$\nu_2^{w} + \nu_1^{w}$ (or ν_3^{w})
1.75	1.75	1.73	1.73	1.73			1.75	$\nu_2^{w} + \nu_1^{w}$ (or ν_3^{w}) $+ \nu_L^{w}$
1.52		1.54		1.52				$2\nu_2^{w} + \nu_1^{w}$ (or ν_3^{w})
1.45	1.48	1.43	1.51	1.49	1.43	1.51	1.45	$2\nu_1^{w}$ (or $2\nu_3^{w}$)
	1.41							$2\nu_1^{w}$ (or $2\nu_3^{w}$)
1.17	1.22	1.16	1.22	1.22		1.24	1.18	$(\nu_1 + \nu_2 + \nu_3)^{w}$

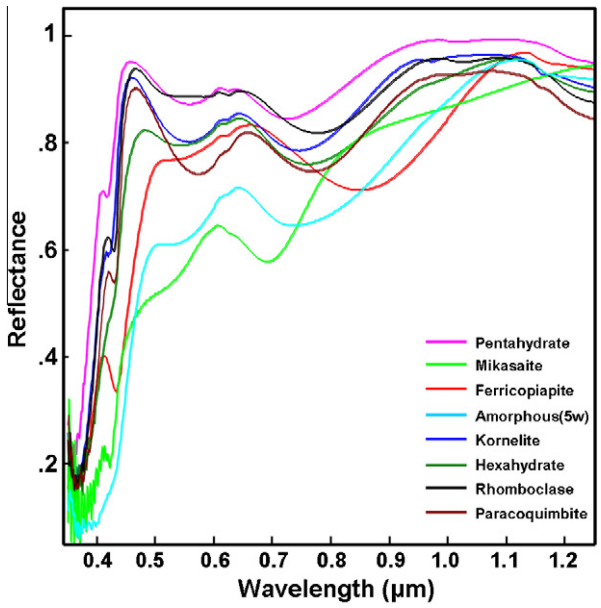

Fig. 5. Vis–NIR reflectance spectra (0.35–1.25 μm) of eight ferric sulfates.

We have observed three trends of major spectral variations among eight ferric sulfates: (1) The absorption band near 0.45 μm due to $^6A_{1g} \rightarrow (4A_{1g}, {}^4E_g$ transition of Fe^{3+} appears to shift towards shorter wavelength (blue-shift) following the decrease of hydration state (0.435 μm for ferricopiapite and 0.424 μm for mikasaite); (2) In the 0.5–0.6 μm region, the absorption feature due to $^6A_{1g} \rightarrow {}^4T_{2g}$ transition of Fe^{3+} varies from a weak absorption shoulder (in the spectra of rhomboclase, amorphous pentahydrate, and ferricopiapite) to become a well-defined absorption band in the spectra of other hydrous phases (especially in the spectra of paracoquimbite and kornelite). Except for ferricopiapite, this band in the spectra of other seven ferric sulfates generally shows a trend of reduction of band-depth and the blue-shift of band center following a decrease of the degree of hydration (0.572 μm for paracoquimbite and 0.531 μm for mikasaite). The distortion of the environments surrounding Fe^{3+} ion in each structure could be the cause but further investigation is needed. (3) In the 0.7–1 μm region, the $^6A_{1g} \rightarrow (4A_{1g}, {}^4E_g)$ transition of Fe^{3+} shows a large blue-shift of band center (0.868 μm for ferricopiapite and 0.703 μm for mikasaite) and the reduction of band width following the decrease of degree of hydration in those ferric sulfates. Notice that the spectrum of amorphous pentahydrate ferric sulfate does not follow all three trends. Also note that the newly found phase hexahydrate ferric sulfate has a major absorption band in 0.7–1 μm region that is broadened and shows a red-shift (towards longer wavelength) from septahydrate (kornelite). The abnormality can be due to a very different lattice environment of Fe^{3+} in this structure, as indicated by the comparison of their Raman spectra (Table 3 and Section 3.3.2), that could produce a slightly different crystal field splitting pattern. The interpretation of spectral features needs further support from the detailed crystal structure refinement of this newly found phase.

A weak band near 1.02 μm was observed in the spectra of rhomboclase, kornelite, and paracoquimbite, which are contributed by high order overtone mode of structural water (listed in Table 6).

Table 6
Center position of absorption bands (in μm) in Vis–NIR spectra (0.35–1.25 μm) for eight synthesized ferric sulfates, and the assignments.

Ferr	Para	Kor	Hex	Pen	Mik	Rhom	Amor	Assignment
0.435	0.429	0.426	0.429	0.420	0.424	0.428	0.433	$^6A_{1g} \rightarrow ({}^4A_{1g}, {}^4E_g)$
0.559	0.572	0.557	0.544	0.559	0.531	0.531	0.558	$^6A_{1g} \rightarrow {}^4T_{2g}$
0.868	0.778	0.755	0.762	0.729	0.703	0.783	0.744	$^6A_{1g} \rightarrow {}^4T_{1g}$
	1.021			1.021		1.028		$3\nu_1^w$ (or $3\nu_3^w$)

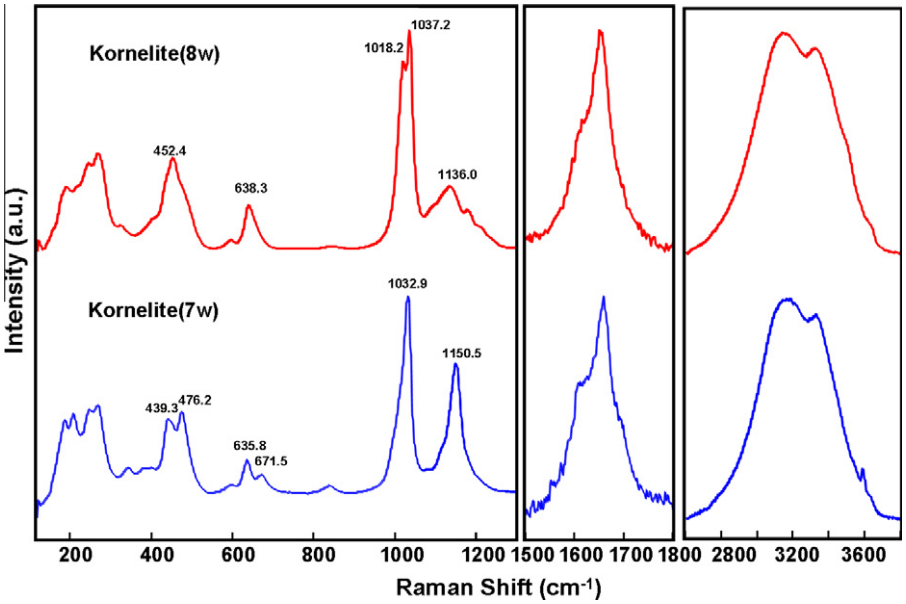

Fig. 6. Comparisons of Raman spectra of kornelite (7w) and the octahydrate ferric sulfate (8w).

3.7. New phenomena observed during the early phase of stability field experiments

We have started 150 sets of experiments, using 10 humidity buffers (from 6% to 100% RH) at three different temperatures (50 °C, 21 °C, and 5 °C), to investigate the stability fields and phase transition pathways of five ferric sulfates (ferricopiapite, kornelite, rhomboclase, crystalline and amorphous pentahydrate). Gravimetric measurements are used to monitor the change of hydration degree, while the phase identification of reaction products at intermediate stages are made by non-invasive Raman spectroscopy using the standard Raman spectra (Fig. 2) obtained during the first step of this series experiments. Results from these 150 sets of experiments will be reported in a following paper. Firstly, we report a few new phenomena observed during the early phase of these experiments.

3.7.1. A potential polymorph of kornelite – an octahydrate ferric sulfate

When the amorphous pentahydrate ferric sulfate was kept in $MgCl_2$ buffer (30.5% RH) at 95 °C, it converted into a new phase in 2 days. Gravimetric measurements indicate that it contains about eight structural water molecules, while the XRD pattern of this new phase agrees with that of kornelite. Nevertheless, there are considerable differences between the Raman spectra of kornelite and this octahydrate ferric sulfate (Fig. 6). Kornelite has a broad v_1 peak at 1032.8 cm^{-1}, while the new octahydrate has a doublet at 1037.2 cm^{-1} and 1018.2 cm^{-1}. The v_2 mode of kornelite splits into two peaks at 439.3 cm^{-1} and 476.2 cm^{-1}, while the v_2 mode of octahydrate (452.4 cm^{-1}) has no splitting. The v_3 mode of kornelite occurs at 1150.5 cm^{-1} with almost equal peak intensity to its v_1 mode, while the corresponding peak (1136.0 cm^{-1}) in the spectrum of octahydrate has only moderate peak intensity and has additional two more minor peaks at the high wavenumber wing of 1136.0 cm^{-1} peak. For the water peaks at 1500–1800 cm^{-1} and 2600–3800 cm^{-1}, the octahydrate has a similar peak shape to that of kornelite, but a larger peak width appears for water stretching modes (region 2600–3800 cm^{-1}), which suggests a higher degree of hydration. Notice in the structure of kornelite, that there are eight crystallographically distinct types of water (named by O_{w1} to O_{w8} in Robinson and Fang (1973)). Among them, six (O_{w1} to O_{w6}) are connected to Fe^{3+} and forming $[FeO_3(O_wH_2)_3]$ octahydra (there are two distinct Fe^{3+} sites), while O_{w7} and O_{w8} do not connect to any Fe^{3+} or any S thus represent two "free" water molecules in kornelite structure (Fig. 1b). This structural character of kornelite leaves the possibility to increase the water content (from seven to eight structural waters) as "free water" without influencing the main structural framework, i.e. without changing the XRD pattern of kornelite. Therefore, we suggest the formation of a potential polymorph of kornelite (with eight structural waters) at 30.5% RH and 95 °C. It is worth noting that this polymorph started to diminish after 3 days at the same RH and *T* conditions, and was totally converted to standard kornelite (confirmed by Raman ID and gravimetric measurement) after 8 days.

3.7.2. Amorphous ferric sulfates with a wide range of degree of hydration

Similar to amorphous Mg-sulfates (Vaniman et al., 2004; Wang et al., 2006a, 2009), the amorphous ferric sulfates are interesting because of their potential to hold large quantities of structural water and their meta-stability in a large temperature range (50–5 °C) at extremely dry conditions that is relevant to Mars.

During some of the 150 experiments for the stability field study with pentahydrated amorphous ferric sulfate as the starting phase (e.g. at 5 °C and 33.6% RH, Fig. 7), we found that amorphous ferric sulfate was able to continuously increase its structural water content but kept its amorphous structure until 11 structural water molecules per formula was reached. The increase of structural water (not adsorbed water) was manifested by the systematic Raman peak position shift to lower wavenumber, from 1134.3 cm^{-1} for amorphous pentahydrate to 1022.1 cm^{-1} that corresponding 11 structural water per formula (by gravimetric measurement at day 54, Fig. 7b), while still keeping a typical Raman spectral pattern of non-crystalline phase (i.e. very large peak width compared with other crystalline ferric sulfates, Figs. 7a and 2). A similar trend of Raman peak position down-shift following the increase of hydration degree was observed for crystalline ferrous sulfates (Chio et al., 2007), Ca-sulfates (Liu et al., 2009) and Mg-sulfates (Wang et al., 2006a, 2009), as well as for amorphous Mg-sulfates (Wang and Freeman, 2009). It was found that amorphous Mg-sulfate can host 1.25–3 structural waters per $MgSO_4$ formula (Vaniman et al., 2004; Wang et al., 2009). We found that the water content range in amorphous ferric sulfate has a much wider range: from 5 to 11 structural waters per $Fe_2(SO_4)_3$ formula. It is worthwhile to note that this red-shift of Raman peak position is nonlinear. When incorporating 5–8 structural waters, the Raman peak

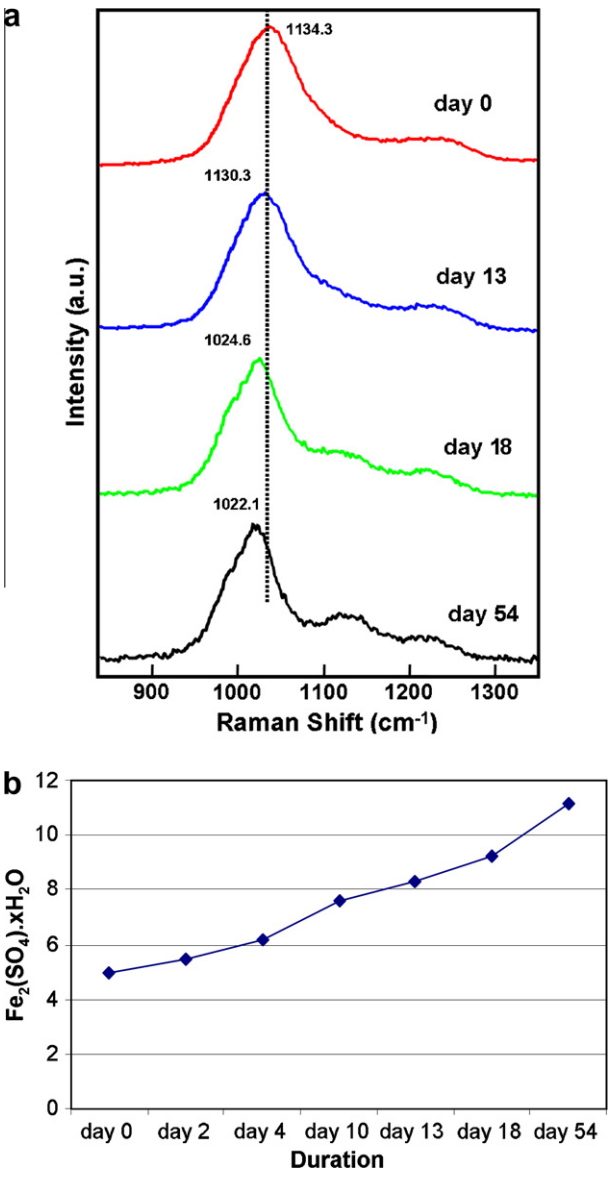

Fig. 7. Wide range of hydration states in amorphous ferric sulfates: (a) hydration state variations revealed by Raman peak position shift; (b) hydration state variations suggested by gravimetric measurements (started from a pentahydrated amorphous phase, at 5 °C and 33.6% RH, in 54 days).

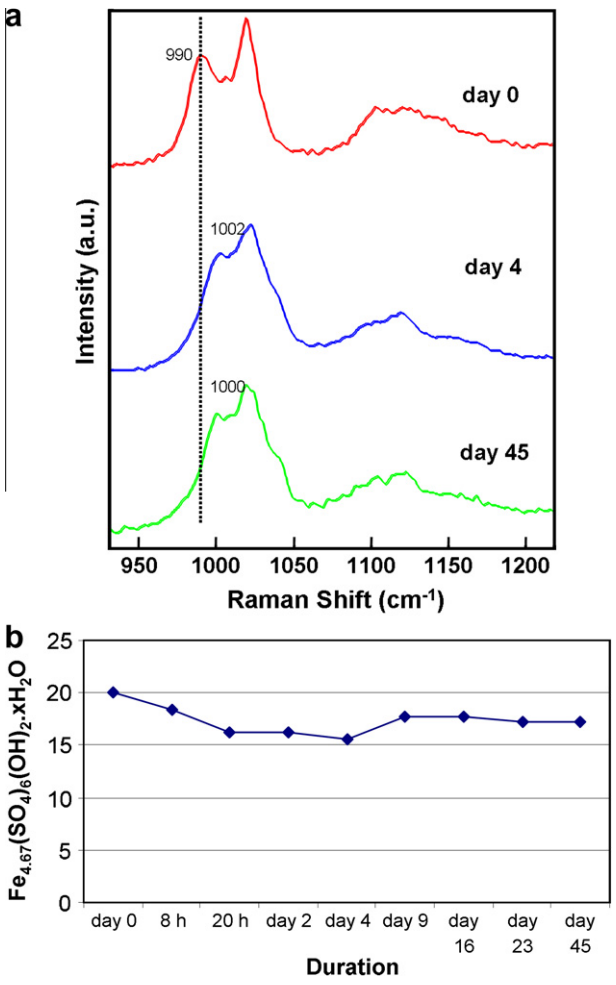

Fig. 8. A wide range of hydration state in ferricopiapite (started from a synthetic ferricopiapite sample, at 50 °C and 5.5% RH, in 45 days): (a) Raman peak position upper-shift following the development of dehydration; (b) loss of structural water molecules per formula during the dehydration by gravimetric measurements.

shift was 4 cm^{-1}; when increasing from eight to nine structural waters, the peak shift jumped to 5.7 cm^{-1}; from 9 to 11 structural waters, the peak shift was 2.5 cm^{-1}. Nevertheless, we can still make a rough estimation on the hydration degree of an amorphous ferric sulfate based on the position of its v_1 Raman peak.

3.7.3. A wide range of hydration degree from a ferricopiapite

Very different from epsomite that holds the highest degree of hydration for Mg-sulfates (above or below 2 °C), ferricopiapite [$Fe_{4.67}(SO_4)_6(OH)_2{\cdot}20H_2O$], that holds the highest degree of hydration among ferric sulfates, has a very large stability (meta-stability) field. It can lose some of its structural water but still keep the same structural framework. This property was evidenced by non-invasive Raman and gravimetric measurements during the stability field experiments. During a dehydration experiment started from ferricopiapite at relatively high temperature and dry conditions (50 °C, 5.5% RH), we noticed that its v_1 Raman peak (Fig. 8) red-shifted from 990 cm^{-1} to 1002 cm^{-1}, and then shifted back to 1000 cm^{-1}, while the general Raman spectral pattern of ferricopiapite was unchanged. This trend of Raman peak shifts was accompanied by gravimetric measurements (on the same samples, Fig. 8b) that show a loss of water from 20 molecules per formula to 15.6 molecules per formula after the first 4 days, then was kept at 17.1 molecules per formula from day nine on. We believe that the capability of keeping a wide range of structural water molecules per formula (from 20 to 15.6) by ferricopiapite is the reason for its stability under a large range of RH–*T* conditions. This capability is given by "free" water molecules (up to 6) in its structure, which only connect to SO_4 tetrahedra and Fe^{3+} centered octahedra by hydrogen bonding. Similar to the "free" water in the kornelite structure (discussed in Section 3.7.1), losing a few "free" waters per formula would not affect the major structural framework of ferricopiapite. Therefore, except for some peak position shifts, there was no major change in its Raman spectral pattern, as observed.

4. On-going experiments

Stimulated by the mission observations (orbital remote sensing and surface exploration) of ferric sulfates on Mars, we are conducting a series of experiments to understand the formation conditions, stability fields, phase boundary and phase transition pathways of these important minerals. Data reported in this paper mark the first step of our investigations, the forming conditions and the structural characteristics of various ferric sulfates, by using a set of spectroscopic technologies that are conventionally used in planetary missions.

The 150 sets of experiments to investigate the stability field and phase transition pathways of five ferric sulfates are still on-going. In addition to the few new phenomena reported here, the final results from those experiments will be reported in another paper and will be compared with some mission observations on Mars.

Acknowledgments

This study was partial supported by NASA Grant NNX07AQ34G. Zongcheng Ling was supported by a special fund established for the collaboration between School of Space Sciences and Physics at Shandong University (PR China) and Dept. Earth and Planetary Sciences at Washington University in St. Louis. Ling also appreciates the support from China Postdoctoral Science Foundation (Grant No. 20090450580), the National High Technology Research and Development Programme of China (No. 2008AA12A212), and the Young Researcher Grant of National Astronomical Observatories, Chinese Academy of Sciences, during the preparation of this manuscript. The authors thank two anonymous reviewers whose constructive comments are very helpful in improving the quality of the paper.

References

Alpers, C., Jambor, J., Nordstrom, D., Ribbe, P., 2000. Sulfate Minerals: Crystallography, Geochemistry, and Environmental Significance. Mineralogical Society of America, Washington.

Arvidson, R.E., Poulet, F., Bibring, J.P., Wolff, M., Gendrin, A., Morris, R.V., Freeman, J.J., Langevin, Y., Mangold, N., Bellucci, G., 2005. Spectral reflectance and morphologic correlations in eastern Terra Meridiani, Mars. Science 307, 1591–1594.

Bibring, J.P., and 11 colleagues, 2005. Mars surface diversity as revealed by the OMEGA/Mars Express observations. Science 307, 1576–1581.

Burns, R., 1993. Mineralogical Applications of Crystal Field Theory. Cambridge University Press.

Chio, C.H., Sharma, S.K., Muenow, D.W., 2007. The hydrates and deuterates of ferrous sulfate ($FeSO_4$): A Raman spectroscopic study. J. Raman Spectrosc. 38, 87–99.

Chipera, S.J., Vaniman, D.T., 2007. Experimental stability of magnesium sulfate hydrates that may be present on Mars. Geochim. Cosmochim. Acta 71, 241–250.

Chou, I.M., Seal, R.R., Hemingway, B.S., 2002. Determination of melanterite–rozenite and chalcanthite–bonattite equilibria by humidity measurements at 0.1 MPa. Am. Mineral. 87, 108–114.

Clark, B.C., Baird, A.K., Weldon, R.J., Tsusaki, D.M., Schnabel, L., Candelaria, M.P., 1982. Chemical-composition of martian fines. J. Geophys. Res. 87, 59–67.

Clark, B.C., and 23 colleagues, 2005. Chemistry and mineralogy of outcrops at Meridiani Planum. Earth Planet. Sci. Lett. 240, 73–94.

Cloutis, E.A., and 11 colleagues, 2006. Detection and discrimination of sulfate minerals using reflectance spectroscopy. Icarus 184, 121–157.

Cloutis, E.A., Craig, M.A., Kruzelecky, R.V., Jamroz, W.R., Scott, A., Hawthorne, F.C., Mertzman, S.A., 2008. Spectral reflectance properties of minerals exposed to simulated Mars surface conditions. Icarus 195, 140–168.

Freeman, J., Jin, M., Wang, A., 2008. D_2O substitution experiment on hydrated iron and magnesium sulfates and its application for spectral interpretation of martian sulfates. Lunar Planet. Sci. XXXVIIII. Abstract #2390.

Freeman, J., Wang, A., Ling, Z., 2009. Ferric sulfates on Mars: Mission observations and laboratory investigations. Lunar Planet. Sci. XXXX, 2284.

Frost, R.L., Wills, R.A., Martens, W., Weier, M., Reddy, B.J., 2005. NIR spectroscopy of selected iron(II) and iron(III) sulphates. Spectrochim. Acta 62A, 42–50.

Gellert, R., and 11 colleagues, 2006. Alpha Particle X-ray Spectrometer (APXS): Results from Gusev Crater and calibration report. J. Geophys. Res. 111, E02S05. doi:10.1029/2005JE002555.

Gendrin, A., and 10 colleagues, 2005. Sulfates in martian layered terrains: The OMEGA/Mars Express view. Science 307, 1587–1591.

Greenspan, L., 1977. Humidity fixed points of binary saturated aqueous solutions. J. Res. Natl. Bureau Stand. – A. Phys. Chem. 81A, 89–96.

Haskin, L.A., and 29 colleagues, 2005. Water alteration of rocks and soils on Mars at the Spirit rover site in Gusev Crater. Nature 436, 66–69.

Hunt, G.R., Ashley, R.P., 1979. Spectra of altered rocks in the visible and near-infrared. Econ. Geol. 74, 1613–1629.

Jerz, J.K., Rimstidt, J.D., 2003. Efflorescent iron sulfate minerals: Paragenesis, relative stability, and environmental impact. Am. Mineral. 88, 1919–1932.

Johnson, J.R., Bell, J.F., Cloutis, E., Staid, M., Farrand, W.H., Mccoy, T., Rice, M., Wang, A., Yen, A., 2007. Mineralogic constraints on sulfur-rich soils from Pancam spectra at Gusev Crater, Mars. Geophys. Res. Lett. 34, L13202. doi:10.1029/2007GL029894.

Klingelhofer, G., and 18 colleagues, 2004. Jarosite and hematite at Meridiani Planum from Opportunity's Mossbauer spectrometer. Science 306, 1740–1745.

Lane, M.D., Bishop, J.L., Dyar, M.D., King, P.L., Parente, M., Hyde, B.C., 2008. Mineralogy of the Paso Robles soils on Mars. Am. Mineral. 93, 728–739.

Langevin, Y., Poulet, F., Bibring, J.P., Gondet, B., 2005. Sulfates in the north polar region of Mars detected by OMEGA/Mars Express. Science 307, 1584–1586.

Lichtenberg, K.A., and 13 colleagues, 2007. Coordinated analyses of orbital and Spirit rover data to characterize surface materials on the cratered plains of Gusev Crater, Mars. J. Geophys. Res. 112, E12S90. doi:10.1029/2006JE002850.

Lichtenberg, K., Arvidson, R., Morris, R., Murchie, S., Bishop, J., Glotch, T., Noe Dobrea, E., Mustard, J., Andrews-Hanna, J., Roach, L., 2009. Stratigraphy and relationship of hydrated minerals in the layered deposits of Aram Chaos, Mars. Lunar Planet. Sci. XXXX. Abstract #2326.

Liu, Y., Wang, A., Freemen, J., 2009. Raman, MIR, and NIR spectroscopic study of calcium sulfates: Gypsum, bassanite, and anhydrite. Lunar Planet. Sci. XXXX. Abstract #2128.

Majzlan, J., Botez, C., Stephens, P.W., 2005. The crystal structures of synthetics Fe-$2(SO_4)(3)(H_2O)(5)$ and the type specimen of lausenite. Am. Mineral. 90, 411–416.

Milliken, R.E., Mustard, J.F., Poulet, F., Jouglet, D., Bibring, J.P., Gondet, B., Langevin, Y., 2007. Hydration state of the martian surface as seen by Mars Express OMEGA: 2. H_2O content of the surface. J. Geophys. Res. 112, E08S07. doi:10.1029/2006JE002853.

Milliken, R.E., and 11 colleagues, 2008. Opaline silica in young deposits on Mars. Geology 36, 847–850.

Ming, D.W., and 16 colleagues, 2006. Geochemical and mineralogical indicators for aqueous processes in the Columbia Hills of Gusev Crater, Mars. J. Geophys. Res. 111, E02S12. doi:10.1029/2005JE002560.

Ming, D.W., and 18 colleagues, 2008. Geochemical properties of rocks and soils in Gusev Crater, Mars: Results of the Alpha Particle X-Ray Spectrometer from Cumberland ridge to home plate. J. Geophys. Res. 113, E12S39. doi:10.1029/2008JE003195.

Morris, R.V., and 19 colleagues, 2006. Mossbauer mineralogy of rock, soil, and dust at Gusev Crater, Mars: Spirit's journey through weakly altered olivine basalt on the plains and pervasively altered basalt in the Columbia Hills. J. Geophys. Res. 111, E02S13. doi:10.1029/2005JE002584.

Morris, R.V., and 16 colleagues, 2008. Iron mineralogy and aqueous alteration from Husband Hill through Home Plate at Gusev Crater, Mars: Results from the Mossbauer instrument on the Spirit Mars Exploration Rover. J. Geophys. Res. 113, E12S42. doi:10.1029/2008JE003201.

Murchie, S., and 49 colleagues, 2007. Compact reconnaissance Imaging Spectrometer for Mars (CRISM) on Mars Reconnaissance Orbiter (MRO). J. Geophys. Res. – Planets 112, E05S03. doi:10.1029/2006JE002682.

Nakamoto, K., 1986. Infrared and Raman Spectra of Inorganic and Coordination Compounds. Wiley, New York.

Rice, M., Bell, J., Cloutis, E., Wang, A., Ruff, S., Craig, M., Bailey, D., Johnson, J., De Souza, P., Farrand, W., 2009. Silica-rich deposits and hydrated minerals at Gusev Crater, Mars. Lunar Planet. Sci. XXXX. Abstract #2134.

Roach, L., Mustard, J., Murchie, S., Weitz, C., Ehlmann, B., Pelkey, S., Seelos, F., Seelos, K., Bibring, J., 2007. Sulfate identification in east candor, Valles Marineris with CRISM visible–infrared spectra. Lunar Planet. Sci. XXXVIII.

Robinson, P.D., Fang, J.H., 1971. Crystal structures and mineral chemistry of hydrated ferric sulphates. 2. Crystal structure of paracoquimbite. Am. Mineral. 56, 1567-1572.

Robinson, P.D., Fang, J.H., 1973. Crystal-structures and mineral chemistry of hydrated ferric sulfates. 3. Crystal-structure of kornelite. Am. Mineral. 58, 535–539.

Ruff, S.W., Christensen, P.R., Blaney, D.L., Farrand, W.H., Johnson, J.R., Michalski, J.R., Moersch, J.E., Wright, S.P., Squyres, S.W., 2006. The rocks of Gusev Crater as viewed by the Mini-TES instrument. J. Geophys. Res. 111, E12S18. doi:10.1029/2006JE002747.

Vaniman, D.T., Chipera, S.J., 2006. Transformations of Mg- and Ca-sulfate hydrates in Mars regolith. Am. Mineral. 91, 1628–1642.

Vaniman, D.T., Bish, D.L., Chipera, S.J., Fialips, C.I., Carey, J.W., Feldman, W.C., 2004. Magnesium sulphate salts and the history of water on Mars. Nature 431, 663–665.

Wang, A., Freeman, J., 2009. Pathways and rates of Mg-sulfate dehydration and rehydration on Mars. Lunar Planet. Sci. XXXX. Abstract #3034.

Wang, A., Freeman, J.J., Jolliff, B.L., Chou, I.M., 2006a. Sulfates on Mars: A systematic Raman spectroscopic study of hydration states of magnesium sulfates. Geochim. Cosmochim. Acta 70, 6118–6135.

Wang, A., and 12 colleagues, 2006b. Sulfate deposition in subsurface regolith in Gusev Crater, Mars. J. Geophys. Res. 111, E02S17. doi:10.1029/2005JE002513.

Wang, A., and 10 colleagues, 2006c. Evidence of phyllosilicates in Wooly Patch, an altered rock encountered at West Spur, Columbia Hills, by the Spirit rover in Gusev Crater, Mars. J. Geophys. Res. 111, E02S16. doi:10.1029/2005JE002516.

Wang, A., and 14 colleagues, 2008a. Light-toned salty soils and coexisting Si-rich species discovered by the Mars Exploration Rover Spirit in Columbia Hills. J. Geophys. Res. 113, E12S40. doi:10.1029/2008JE003126.

Wang, A., Ling, Z., Freeman, J., 2008b. Ferric sulfates on Mars: Surface explorations and laboratory experiments. American Geophysical Union, Fall Meeting 2008. Abstract #P44A-08.

Wang, A., Freeman, J.J., Jolliff, B.L., 2009. Phase transition pathways of the hydrates of magnesium sulfate in the temperature range 50 °C to 5 °C: Implication for sulfates on Mars. J. Geophys. Res. 114, E04010. doi:10.1029/2008JE003266.

Wiseman, S.M., and 15 colleagues, 2008. Phyllosilicate and sulfate–hematite deposits within Miyamoto crater in southern Sinus Meridiani, Mars. Geophys. Res. Lett. 35, L19204. doi:10.1029/2008GL035363.

Yen, A.S., and 13 colleagues, 2008. Hydrothermal processes at Gusev Crater: An evaluation of Paso Robles class soils. J. Geophys. Res. 113, E06S10. doi:10.1029/2007JE002978.